Spatially decaying turbulence and its relation to mixing across density interfaces

By E. J. HOPFINGER AND J.-A. TOLY

Laboratoire de Mécanique des Fluides (Laboratoire Associé au C.N.R.S.),
Université de Grenoble, France

The turbulence generated by a vertically oscillating grid in a water tank and the entrainment across a salinity interface caused by this turbulence have been investigated experimentally. Measurements were carried out in a homogeneous layer of fluid as well as a two-layered fluid, which permitted us to determine the decay law of this turbulence and the way in which the structure of the turbulence depends on the mesh size and on the frequency and amplitude of the grid oscillation. It was found that the turbulent kinetic energy decays with distance from the grid according to a power law $\overline{q^2} \propto z^{-n}$, with n close to 2, and that the turbulent Reynolds number remains approximately constant during decay. The linear dependence of the r.m.s. turbulent velocity on the grid oscillation frequency found by Thompson & Turner (1975) in the case of a square-bar grid has been confirmed. It is shown here that this linear relation remains valid when an interface is present and consequently the dependence of the entrainment velocity on the local Richardson number is of the form $u_e/u \propto Ri^{-\frac{3}{2}}$, the Péclet number being high. While the bearing of these results on the problem of the thermocline or an inversion is clear we wish to emphasize that the spatial decay of turbulence is interesting in itself.

1. Introduction

The existence of relatively sharp density interfaces in the ocean, the atmosphere and lakes is now well documented. Since these interfaces control or inhibit the vertical transport of energy and mass it is desirable to predict their location and to have a good knowledge of the exchange processes involved. Small-scale laboratory experiments have been very helpful and the situation where the mixing process is driven by externally, mechanically generated turbulence has been simulated in two ways: first, by generating turbulence by oscillating a grid vertically in one layer of a two-layered fluid (Rouse & Dodu 1955; Turner 1968) or in a linearly stratified fluid (Linden 1975); second, by imposing a stress by means of a moving screen (Kato & Phillips 1969) or an air stream (Wu 1973) on the free surface of one layer or a linearly stratified layer. The stress produced by these laboratory means and the wind stress alike generate both turbulence and a mean flow. But the mechanism of turbulence generation by wind stress (which is not well understood) may be different from that of the laboratory stress models. In particular, in the latter, the turbulence in the well-mixed layer has a scale

which is related to the layer depth, whereas in the former turbulence may be largely caused by the breaking of surface waves, in which case its structure would bear no direct relation to the mixed-layer depth (Turner 1973, p. 292). This independence of the structure of the turbulence of the location of the interface is characteristic of turbulence generated by oscillating grids or by a turbulent plume impinging on an interface (Baines 1975).

Regardless of the prevailing structure in nature, useful information has been obtained from both types of experiment, and idealized situations like the projection of vortex rings against a density interface (Linden 1973) have revealed basic features of the mixing process. The shear and grid experiments have, however, led to a different functional dependence of the non-dimensional entrainment velocity u_e/u_* (u_* is a velocity scale of the generating mechanism) on the global Richardson number Ri^* and this is rather perplexing. The results of the former seem† to be consistent with $u_e/u_* \propto Ri^{*-1}$, which implies that the potential energy gained is proportional to the kinetic energy supplied, whereas the latter support such an energy argument only when the Péclet number $Pe = ul/\kappa$ (where u is the r.m.s. horizontal velocity, l the integral length scale and κ the diffusivity) is small; at high Péclet numbers $u_e/u_* \propto Ri^{*-\frac{3}{2}}$. This behaviour of the grid experiments at high Péclet numbers is supported by the plume experiments carried out by Baines. Long (1975) suggested that the $Ri^{*-\frac{3}{2}}$ law is not fundamental (contradicting Linden's 1973 conclusion) and that the different behaviour might simply be due to the existence of a weak density gradient in the mixed layer which affects the proportionality between the energy available at the interface and the energy supplied by the stirrer. In other words, the local Richardson number Ri, defined using the local turbulence scales, would not remain proportional to Ri^*. This controversy makes it clear that a realistic comparison of these different experimental results and their confrontation with the situation in nature will only be possible if the structure of the turbulence near the interface is known.

A first step in this direction has been made by Thompson & Turner (1975), who measured the r.m.s. turbulent velocity and the length scale at various levels in the box used by Turner (1968) but without any interface. Similar measurements have been carried out by Bouvard & Dumas (1967), who used as the stirrer a perforated plate rather than a grid and attained turbulent Reynolds numbers Re_l (based on the integral scale) of about 6×10^3. The spatial‡ decay of the horizontal r.m.s. turbulent velocity u is not the same in the two experiments although Thompson & Turner tried to interpret their results in the light of those of Bouvard & Dumas. Thompson & Turner's results support the existence of Reynolds number similarity, i.e. $ul/\nu =$ constant, whereas the perforated-plate results indicate a non-uniform decrease in the turbulent Reynolds number with distance from the stirrer. Furthermore, Thompson & Turner found that the results corresponding to their grid of square bars are consistent with proportionality between the r.m.s. turbulent velocity at a fixed level and the stirrer frequency f; this is not

† The experimental scatter is considerable and the range of Ri^* rather small, so that the conclusion is somewhat ambiguous.

‡ Note that this problem is quite different from the time-decay problem.

the case for the perforated plate, for which u increases less rapidly than f (Toly 1975).

In this paper the decay law is re-examined in the light of new experimental results obtained in the box of Bouvard & Dumas but using as the stirrer different grids made of square bars. The way in which the turbulent length and velocity scales can be changed by varying the mesh size and the stroke has been made clear. This is of interest in mixing studies. These results are completed by measurements of the entrainment rate and turbulence quantities when a density interface is present. While the importance of the study in the geophysical context has been made clear, we wish to emphasize its fundamental interest in turbulence. It permits isolation of the diffusion terms in the turbulent energy equation in a unique way and determination of the *spatial* decay of turbulence with planar homogeneity.

2. Experimental arrangement

2.1. *Installation*

The installation used was the one constructed by Bouvard & Dumas (1967). It is a box of dimensions $67 \cdot 5 \times 67 \cdot 5$ cm (or 80×80 cm; see figure 1) and height 1 m. The stirrers employed were grids made of square bars having mesh sizes $M = 5$ and 10 cm with $M/d = 5$. The configuration used in most of the experiments reported here is shown in figure 1 (b). The grids were made rigid by a frame and placed about 45 cm above the bottom of the box. This height was found to be necessary in order to reduce the secondary motion to an acceptable level. The measurements were made in the layer above the grid only. For the sake of direct comparison, some experiments were run with the perforated plate used by Bouvard & Dumas, placed at about 20 cm above the bottom. In the initial grid experiments the grids were also at this height, but this configuration caused strong secondary motions in the four corners which modified the decay law considerably (see §4.4). An attempt to isolate a central section of the flow field by inserting a bottomless inner box as shown in figure 1 (a) did not eliminate the secondary motion, completely, especially with a mesh size of 10 cm. Measurements were carried out for stirrer frequencies between 2 and 6 Hz and strokes of 4 and 9 cm. Thompson & Turner (1975) used a 1 cm stroke.

2.2. *Measurement techniques*

The measurements of the turbulent quantities were carried out mainly with a hot-film probe mounted on a rotating spindle. A laser anemometer was used to check the hot-film results. The measurements were made with a conical probe except in some cases where an X-probe had to be used. The arm on which the probe is mounted is 19 cm long and causes a bulk rotation of the fluid which becomes significant after a certain time of operation. Since the spin-up time is generally much greater than the integration time it was possible to stop the spindle rotation before the fluid rotation caused any problems. The angular velocity was chosen such that the wake remained small but unfortunately not
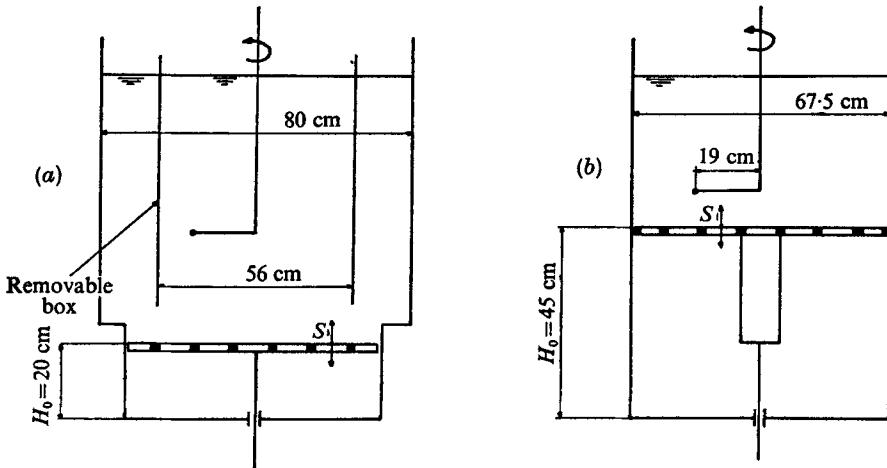
FIGURE 1. Schematic diagram of the experimental installation.

insignificant when the turbulent velocity was small, i.e. when working at low frequencies or far away from the stirrer. Corrections of the form $\overline{u^2_{\text{turb}}} = \overline{u^2} - \overline{u^2_{\text{wake}}}$ were applied to all the measurements. Here $\overline{u^2_{\text{wake}}}$ was determinated in the non-agitated fluid and its numerical value was generally close to $0\cdot3$ cm^2/s^2, which includes irregularities in the probe rotation and noise. For comparison, the lowest r.m.s. turbulent velocities measured were $0\cdot7$ cm/s. In the corrections used it was supposed that the correlation $\overline{u'_{\text{turb}}\, u'_{\text{wake}}}$ is negligible and that the wake energy measured in the non-agitated fluid differs little from the $\overline{u^2_{\text{wake}}}$ in the presence of ambient turbulence. The first assumption was supported by a spectral analysis and some idea of the validity of the second can be obtained when the probe rotation period $2\pi/\Omega$ (where Ω is the angular velocity) is compared with the turbulent diffusion time scale. In the time $2\pi/\Omega$ the grid turbulence would diffuse the wake by roughly $w(2\pi/\Omega)$. When the r.m.s. turbulent velocity is low, i.e. when the wake energy becomes important, this diffusion length is of the same order as the wake dimension in the non-agitated fluid; at higher r.m.s. velocities the wake energy in the turbulent case diffuses faster and hence the corrections made are somewhat exaggerated. Dye injection at the probe tip confirmed these conjectures qualitatively. Since the importance of the corrections depends on the r.m.s. velocity an incorrect correction would particularly affect the functional dependence of u on the stirrer frequency f. Without any correction $u \propto f^m$, with $m < 1$ ($m = 0\cdot7$–$0\cdot8$), whereas with the corrections applied in the way indicated above $u \propto f$. This linear relation is in agreement with Thompson & Turner's (1975) results and it was also verified by means of the laser anemometer† (see figure 12). In spite of this carefully applied correction the accuracy is somewhat affected by the presence of the wake and the experimental error in u is $\pm 5\%$, increasing to about 10% when $\overline{u^2_{\text{wake}}} > 0\cdot1\, u^2_{\text{turb}}$. It was hoped to use the laser anemometer when an interface was present. Unfortunately, no satisfactory

† This anemometer has been developed in our laboratory by Lismonde (1976).

results could be obtained in this case since the mixed layer was only quasi-homogeneous and the salinity fluctuations, although small, caused variations in the refractive index and thus fluctuations of the light beams. In the interface itself, the bending of the laser beam gave useful information about the thickness of the interface.

A Schlumberger CNTR 1024 correlator connected with a Fourier transformer was used for the signal analysis, in particular for the determination of the integral scale and the Taylor microscale. This system has a low cut-off frequency of 0·2 Hz and the sampling frequency in real time is 4 kHz. Generally, the r.m.s. turbulent velocity was obtained by means of a true integrating voltmeter. Since the laser-anemometer signal contained a considerable amount of energy at frequencies situated below the cut-off frequency of some of the instruments used, the signal was recorded and played back at a higher speed.

The entrainment rate as a function of time in the homogeneous case was obtained from photographs of the turbulent/non-turbulent interface made visible by adding rhodamine B to the turbulent fluid. Generally a vertical slice of fluid about 1 cm thick was illuminated for this purpose and photographs were taken at fixed time intervals. When a density interface was present the mixing rate was determined directly by withdrawing fluid at a constant rate, attempting to keep the interface at a given height. The residual changes in height, being of the order of a few millimetres, were measured by means of a cathetometer after the stirrer had been stopped and the interface had levelled out.

3. Mechanisms of turbulence generation

The mechanism of turbulence generation by oscillating grids has already been discussed in detail by Thompson & Turner (1975). We just want to make some complementary remarks and compare the grid mechanism with that of the plate. In the latter case jets are formed above the holes (figures 2b, plate 1), whereas a grid creates a wake behind the bars (figure 2a, plate 1). Since the solidity of the plate is high (60 %) the velocity in the holes exceeds the velocity of the plate, so that the turbulence will originate predominantly in these jets. In the case of grids which have the usual solidity ($< 40\%$) the pockets of turbulence are aligned with the bars and very probably have the structure of wakes on either side; the final turbulence is a result of wake interaction. The spectrum of the wake structure 2 cm above the top position of the grid with $M = 5$ cm for $S = 4$ cm shows two distinct peaks, one at the stirrer frequency and the other at some higher frequency (figure 3). The Strouhal number of the eddies shed behind a fixed square-bar grid placed in a uniform stream is close to 0·2. The Strouhal number based on the frequency of the second peak, $N = 8$ Hz, has the value $St = Nd/\pi Sf = 0·21$. On the other hand the corresponding spectral curve for the grid with $M = 10$ cm for $S = 4$ cm (figure 4) has only one distinct peak. Indeed in this case the shedding frequency coincides with the stirrer frequency. Taking $St = 0·2$ it is easily found that in order for the shedding frequency to be larger than the stirrer frequency it is necessary that $S/d > 2, (S/M > 0·4)$. It may be expected that the structure is amplitude dependent as long as $S/d < 2$. The experimental results
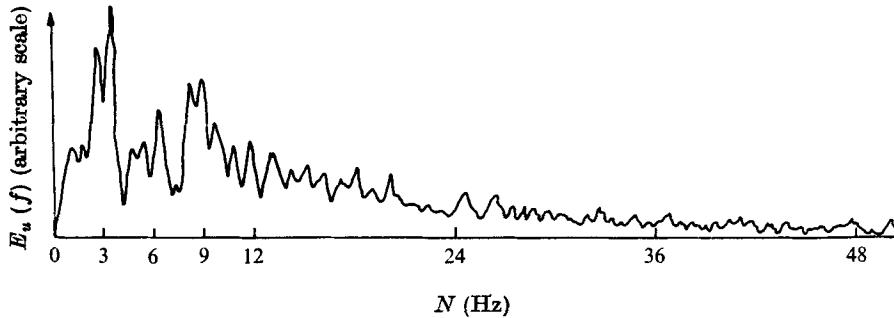
FIGURE 3. Spectrum of the motion 2 cm above the top position of the grid with $M = 5$ cm operated at a stroke $S = 4$ cm and a frequency of 3 Hz. The probe moves at a constant velocity $U = 47$ cm/s.
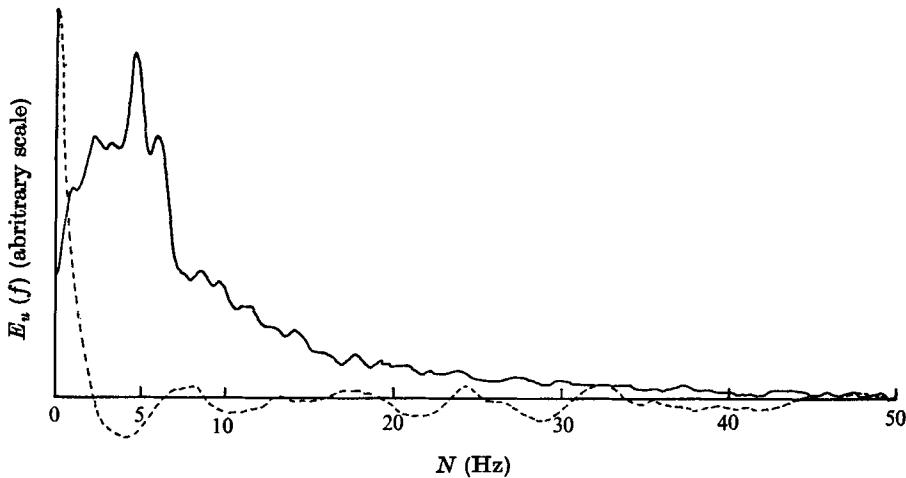
FIGURE 4. Spectrum of the motion 2·5 cm above the top position of the grid with $M = 10$ cm operated at a stroke $S = 4$ cm and a frequency of 5 Hz. $U = 48$ cm/s. ----, auto-covariance $\overline{u'(t)\, u'(t+\tau)}$.

show such a dependence unless $S/d \gtrsim 4$. For both grids the spectra no longer show such distinct peaks 7–8 cm above the top position of the grid. The same behaviour was found by Thompson & Turner. For the perforated plate no such spectra were obtained.

4. Characteristics of oscillating-grid turbulence

4.1. *Dependence of the r.m.s. turbulent velocity on the frequency and stroke of the stirrer*

Measurements of the turbulent velocities were carried out at various distances from the generating grid. In figure 5 the measured r.m.s. horizontal turbulent velocities u are presented in non-dimensional form for the grids with $M = 5$ cm and $M = 10$ cm (keeping $M/d = 5$) for $S = 4$ cm and frequencies between 2 and
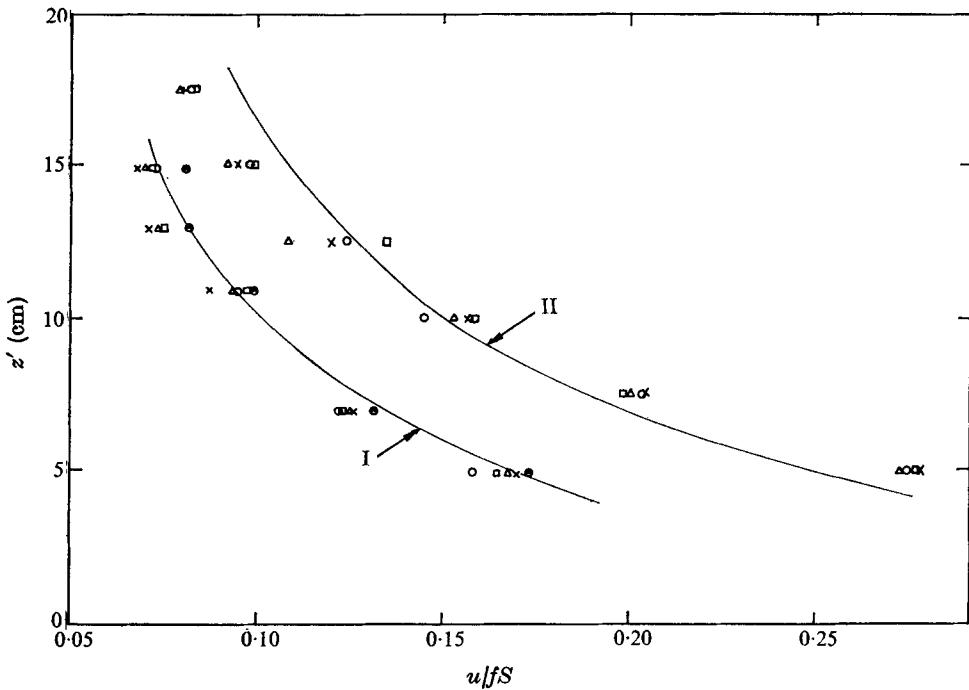
FIGURE 5. Variation of the non-dimensional r.m.s. horizontal turbulent velocity with distance from the grid; z' is measured from the top position of the grid. Curve I, $M = 5$ cm, $S = 4$ cm; curve II, $M = 10$ cm, $S = 4$ cm. ——, curves calculated with $u/fS = Cz^{-1}$ (z measured from the virtual origin); $\square$, $f = 6$ Hz; $\bigcirc$, $f = 5$ Hz; $\triangle$, $f = 4$ Hz; $\times$, $f = 3$ Hz; $\bullet$, $f = 2$ Hz.

6 Hz. Here z' is measured from the top position of the grid;[†] the 'virtual origin' used in the power law $u/fS = $ constant $\times z^{-1}$, plotted for comparison, is here 3 cm below the top position (see §4.3 for the determination of this virtual origin). Since the frequency is the only variable parameter in this set of data, a linear dependence of u on the stirrer frequency is indicated at all depths. The perforated-plate data, on the other hand, seem to approach such a linear dependence only at high stirrer frequencies. For the plate the exponent m in $u \propto f^m$ is less than 1 (whereas Thompson & Turner found $m = \frac{4}{3}$ for a round-bar grid). When $m \neq 1$ an additional variable with units involving time is required for dimensional reasons in the velocity/frequency relation, and viscosity seems to be the only such variable. Viscosity may enter by way of the dependence of the Strouhal number on Reynolds number. In the case of square bars the separation point is well defined and the effective diameter is equal to the true bar diameter, resulting in a Strouhal number which is independent of Reynolds number. The separation point for round bars, on the other hand, is less well defined and remains weakly dependent on Reynolds number even at relatively high Reynolds number. Here the grid Reynolds number is 10^2–10^3. In general we have for u at any plane z

$$u/fS = F(SfM/\nu, S/M)$$

† We refer here to the upper face of the grid, with the grid in its top position.
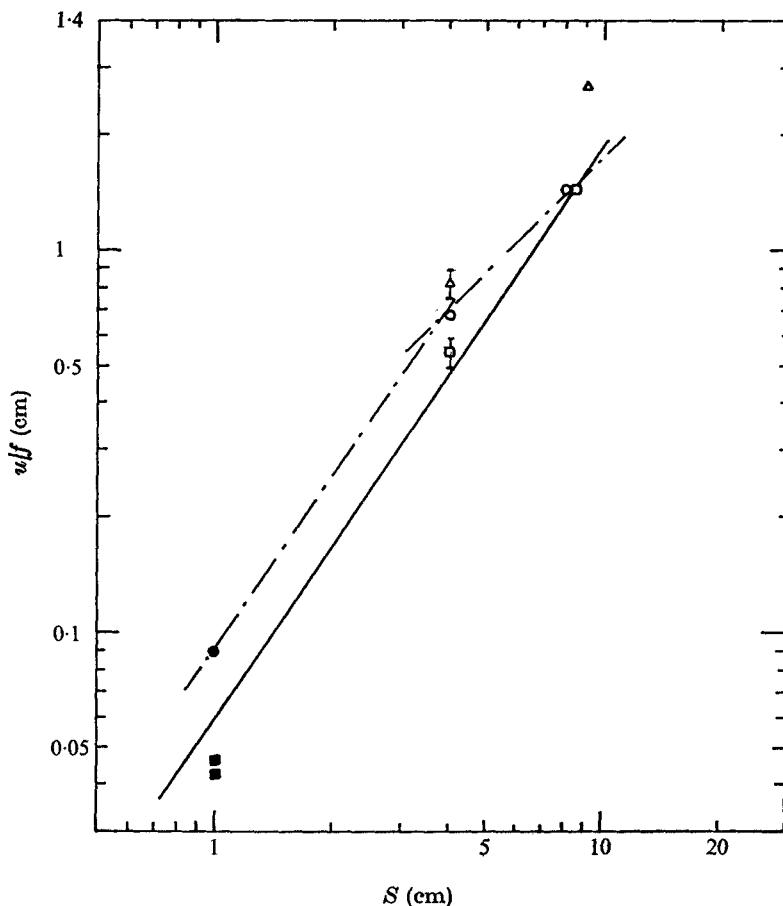
FIGURE 6. Dependence of u/f on the stroke S. z is measured from the virtual origin and z' from the top position of the stirrer. $\square$, $M = 5$ cm, $z = 10$ cm; $\bigcirc$, $M = 5$ cm, $z' = 5$ cm; $\triangle$, $M = 10$ cm, $z = 10.5$ cm; $\blacksquare$, $M = 5$ cm, $z = 10$ cm, from Thompson & Turner (1975); $\bullet$, $M = 5$ cm, $z' = 5$ cm, from Thompson & Turner (1975).

(keeping M/d fixed) and since $u \propto f^m$ it is possible to write

$$u/fS = (SfM/\nu)^{m-1} G(S/M).$$

When square bars are used $m = 1$ and it remains to find the function G. This stroke dependence is more difficult to establish than the frequency dependence. One simple reason is that the stroke is not as easily varied as the frequency, but the main difficulty lies in the choice of the origin. It is possible to compare r.m.s. velocities either at a fixed distance from the top position of the stirrer or at distances referred to the virtual origin. Both possibilities are shown in figure 6, where u/f is plotted logarithmically as a function of the stroke. When the top position is taken as the reference plane two distinct regions seem to be indicated where the transition takes place at $S/d \approx 4$, ($S/M \approx 0.8$). When taking the virtual origin as the reference level the experimental results for one grid geometry are
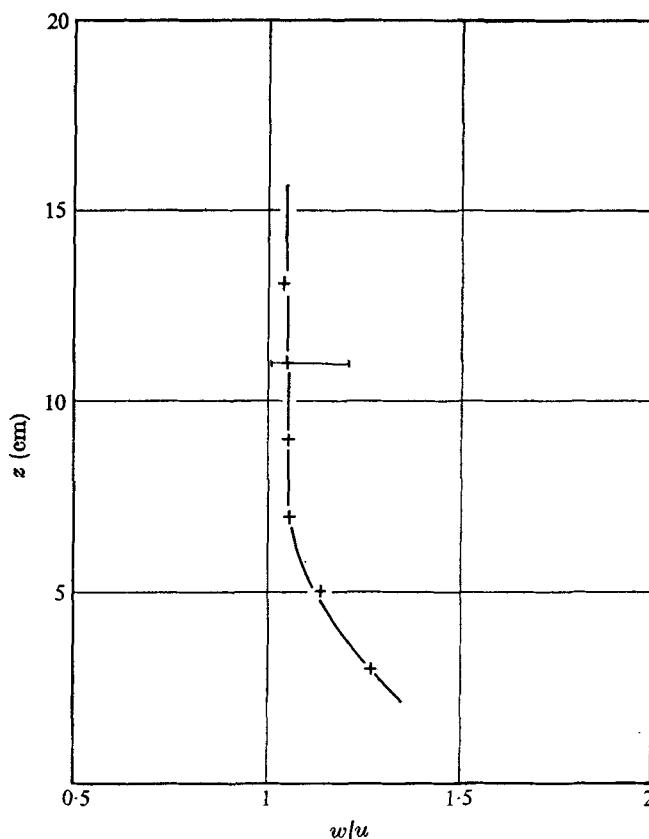
FIGURE 7. Evolution of the degree of isotropy, represented by w/u, with distance z' for the grid with $M = 5$ cm for $S = 4$ cm.

reasonably well represented by $u/f \propto S^{\frac{3}{2}}$. For the grid with $M = 10$ cm, keeping $M/d = 5$ as before, higher values of u are obtained, indicating a dependence on the bar diameter or M. We shall come back to this in §5.

4.2. *Evolution of the degree of isotropy*

The evolution of the degree of isotropy of the turbulence is important to know, since it influences the decay law determined using only the measured r.m.s. horizontal velocity. In other words it is assumed that u^2 is proportional to the turbulent kinetic energy. Figure 7 shows the ratio of the vertical and horizontal turbulent velocities as a function of distance from the grid. Near the grid w is considerably larger than u but only 6–7 cm (corresponding to less than $1 \cdot 5\,M$) away from the grid the turbulence produced by the oscillating grid is roughly isotropic. The values given in figure 7 have been calculated with $\gamma = \alpha \tan \phi$ in $e = \alpha u' + \gamma w'$† ($\phi$ is the angle of the film with respect to the horizontal). A more realistic expression for γ is

$$\gamma = \alpha \tan \phi \left(\frac{1 - k^2}{1 + k^2 \tan^2 \phi} \right)$$

† Here α and γ are the sensitivities for u' and w' respectively.

with $k = 0.03$–0.3 (Resch & Leuchtheusser 1972). This would increase the value of w by at most a factor of 1.2. There is thus some uncertainty concerning the numerical value of w/u but what is important is the fact that w/u remains constant beyond $z_h' = 6$–7 cm (at least within experimental error). The characteristic time of homogenization τ_h is then z_h'/w and this time should be compared with $\tau_t \sim l/u$. The experimental results show that $\tau_h \sim 4\tau_t$ or $z_h' \sim 4l$. Behind a fixed grid $\tau_h \approx 10M/u$ and $\tau_t \sim \frac{1}{4}M \times 10/u$, which gives the same ratio. Note that in the oscillating-grid turbulence $z_h' \propto M$ only when $l \propto M$.

4.3. *Variation of the length scales and the Reynolds number with distance from the stirrer*

The longitudinal integral scales at various distances from the grid have been obtained from the autocovariance of the velocity signal. In all cases the scale is proportional to the distance. The coefficient of proportionality depends on the mesh size and also on the stroke as long as $S/M < 0.8$. Indeed the scale tends to be proportional to M only when $S/M \gtrsim 0.8$. The different results obtained are shown in figure 8 and in table 1, which also contains the microscale determined from the spectra. In figure 8 the results of Thompson & Turner (1975) and of Bouvard & Dumas (1967) are included for comparison. These two sets of data are represented by one curve purely by coincidence and in fact the former measured the longitudinal scale as we did whereas the latter measured the transverse scale. It is evident that the scale obtained by Thompson & Turner for $M = 5$ cm and $S/M = 0.2$ is about one-third of the scale obtained with the same grid but with $S/M = 0.8$.

A 'virtual or effective origin' is obtained by extrapolation of the integral scale to zero. This origin is crucial to the determination of the exponent in the power law of decay. The procedure was to plot l *vs.* z' on a linear scale and fit a straight line to the data. The ordinate value when $l = 0$ is taken as the virtual origin. This origin falls below the top position of the grid by $z_0' = (\frac{1}{2}S + 1 \text{ cm}) \pm 0.5$ cm. It thus falls slightly below the midplane of grid oscillation (here we refer to the centre-plane of the grid) or coincides with it (when $S = 4$ cm and $d = 2$ cm for example). In the case of the perforated plate Bouvard & Dumas's (1967) results lead to $z_0' = \frac{1}{2}S + 2.5$ cm, which is also only slightly below the midplane of oscillation. A virtual origin can also be obtained by fitting the r.m.s. turbulent velocity as a function of z' by a longest straight line. The two effective origins should coincide.

The Reynolds number Re_l is plotted logarithmically in figure 9 as a function of z measured from the virtual origin. Re_l remains practically constant during decay when grids with $M = 5$ cm and $S = 4$ cm or $M = 10$ cm and $S = 9$ cm are used ($S/M \gtrsim 0.8$). However, when the grid with $M = 10$ cm is operated at a stroke $S = 4$ cm, the Reynolds number decreases over the first 20 cm and then remains constant. This behaviour is similar to that for the perforated plate, but in the latter case Re_l decreases more rapidly before reaching an almost constant value sufficiently far away from the stirrer. A plausible explanation for this non-monotonic decrease of Re_l is the possible generation of an unstable turbulent flow by a stirrer of high solidity. Behind a fixed grid the regular array of wakes (or jets) merge without shifting their axes laterally only when the solidity is sufficiently
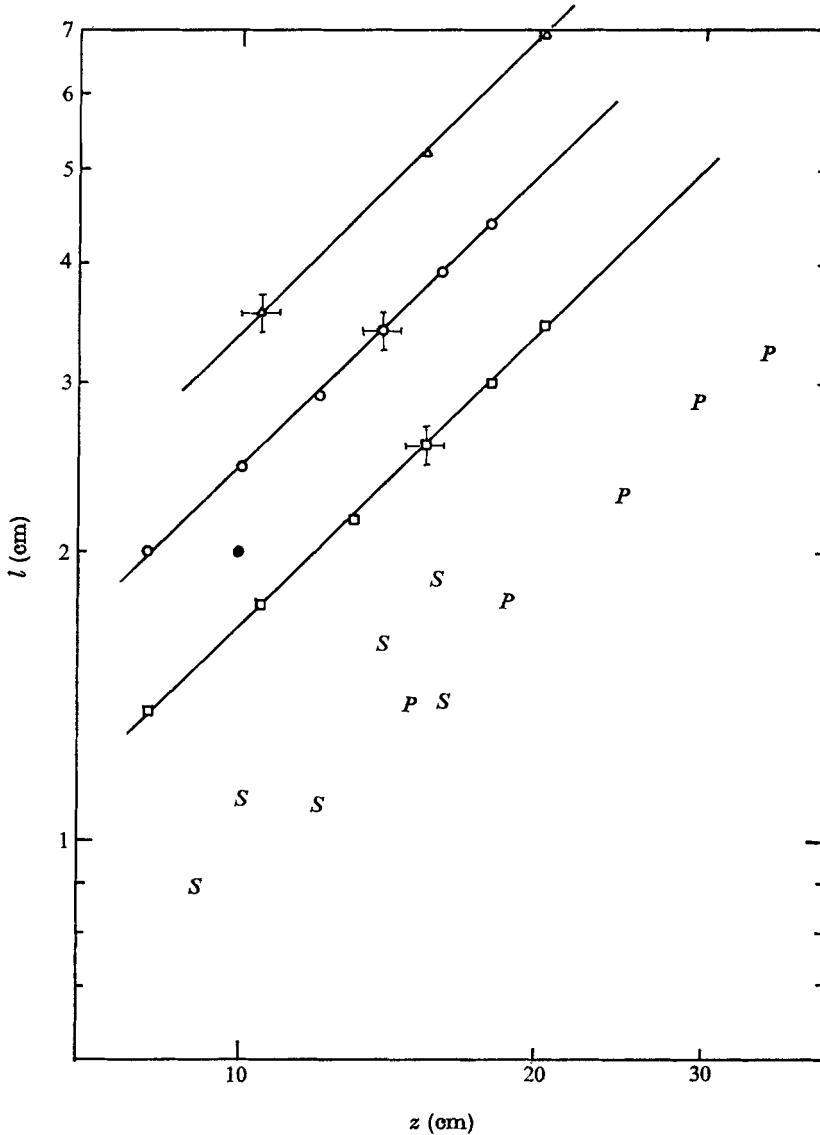
FIGURE 8. Integral length scales plotted logarithmically against distance z. The scales correspond to the longitudinal integral scale except for the perforated plate, in which case the transverse scale of the horizontal velocities was measured. S; square-bar grid of Thompson & Turner (1975); P, perforated plate used by Bouvard & Dumas (1967); $\triangle$, $M = 10$ cm, $S = 9$ cm; $\square$, $M = 10$ cm, $S = 4$ cm; $\bigcirc$, $M = 5$ cm, $S = 4$ cm; $\bullet$ $M = 5$ cm; $S = 8$ cm.

low (Corrsin 1963). When the solidity is too high the wakes or jets are unstable and coalesce successively into larger and larger jets. Both the length scale and its r.m.s. value are affected by this jet switching. The solidity above which this jet switching is observed is about 40 %. It should also be noted that the fluid-dynamical solidity is not necessarily the same as the geometrical solidity.

M	S (cm)	f (Hz)	z (cm)	u (cm/s)	l (cm)	Re_l	λ (cm)	Re_λ
5	4	6	8	4·10	2·00	820	0·34	139
5	4	6	10	3·20	2·44	780	0·43	136
5	4	6	12	2·75	2·92	805	0·51	139
5	4	6	14	2·28	3·41	780	0·60	136
5	4	6	16	1·99	3·92	780	0·69	136·5
5	4	6	18	1·80	4·40	792	0·77	138
5	8	5	10	7·33	2·00	1466	—	—
10	4	6	8	6·66	1·36	906	0·22	147
10	4	6	10·5	4·90	1·76	862	0·29	143·5
10	4	6	13	3·80	2·16	820	0·37	140
10	4	6	15·5	3·00	2·60	780	0·46	137
10	4	6	18	2·35	3·00	705	0·55	130
10	4	6	20·5	1·92	3·44	660	0·65	127
10	9	5	10·5	13·50	3·55	4800	0·24	328
10	9	5	15·5	8·25	5·24	4340	0·38	316
10	9	5	20·5	6·52	6·90	4500	0·50	328

TABLE 1. Numerical values of the r.m.s. horizontal velocity, the length scales and the corresponding Reynolds numbers at various distances from the grid. For the grid with $M = 10$ cm and $S = 4$ cm the r.m.s. velocity was measured up to a distance of 33 cm but the values are not listed here.
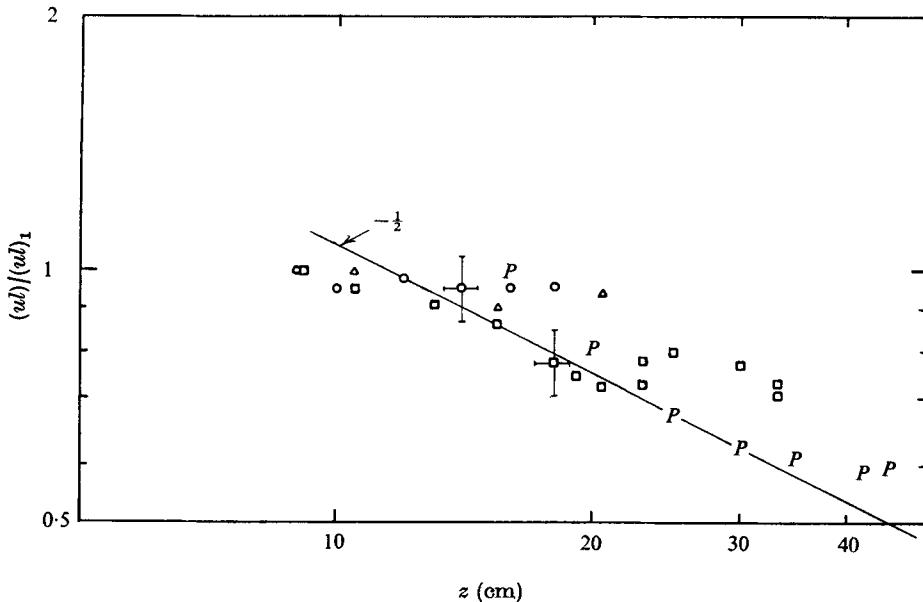

FIGURE 9. Turbulent Reynolds number Re_l plotted logarithmically as a function of z. The corresponding numerical values of other parameters, including Re_λ, are given in table 1. The symbols are explained in figure 8 and the value $(ul)_1$ is the first value given in table 1. The values of Re_l beyond $z = 20·5$ cm have been determined using the extrapolated values of l.
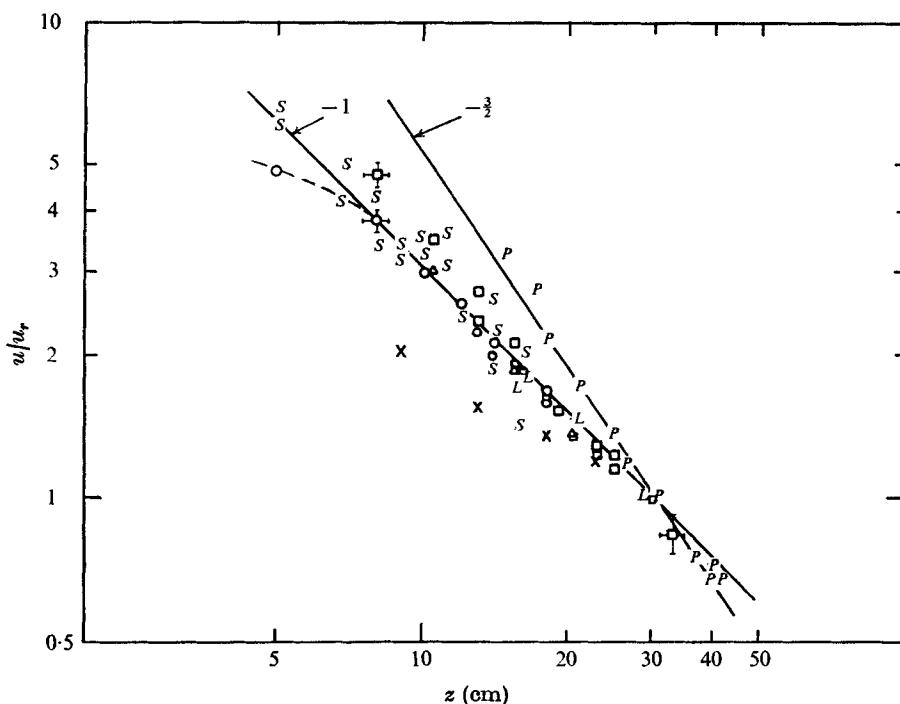
FIGURE 10. R.m.s. horizontal velocity plotted logarithmically against distance z. The crosses correspond to the situation with important secondary motions and the L's are the laser-anemometer results. All other symbols are the same as in figure 8. u_r is the reference velocity at $z = 30$ cm and has the following values.

	$\triangle$	$\square$	$\bigcirc$	S	P	$\times$	L
u_r (cm/s)	4·45	1·40	1·07 (extr.)	0·08 (extr.)	9·75	2·5 (extr.)	1·40

Since $l = \beta z$ in all cases (β being a constant) the variation of the Reynolds number immediately gives the exponent in the power law governing the spatial decay. It is seen that this exponent is close to -1 when $S/M \gtrsim 0.8$, attaining a mean value of about -1.25 in the case of the grid with $M = 10$ cm for $S = 4$ cm. The decay law $u \propto z^{-\frac{3}{2}}$ fitted to the plate data by Thompson & Turner corresponds to $Re_l \propto z^{-\frac{1}{2}}$. The overall decrease is represented by this power law but it would be more appropriate to consider two distinct regions rather than to fit one curve to it. The existence of two distinct regions can also be inferred from the evolution of the transverse length scales measured by Bouvard & Dumas with horizontally separated probes and also with vertically separated probes. The scales were found to be identical beyond about 25 cm, measured from the top position of the plate ($z = 31$ cm in figure 9), and then began to diverge. This transition is in agreement with the transition in the Reynolds number variation and implies a possible change in the state of the turbulent motion.

4.4. *Effects of large-scale motion*

When the inner box was removed from the configuration shown in figure 1 (*a*), the apparent turbulent intensity was considerably increased (by a factor of 1·5–2 depending on the distance from the grid) and the decay is represented by a power

law with an exponent considerably less than 1 (close to 0·5; see figure 10). In fact a closer examination showed that these results could be superposed on the measured r.m.s. turbulent velocities without significant secondary motion by a simple translation of the u axis and a small correction in the origin, in other words by subtracting from the measured values the secondary motion or large-scale motion, which had the same value at all distances, and by shifting the virtual origin down by only 2 cm. The true turbulent motion again decays according to the power law $u \propto z^{-1}$ but the bulk motion does not. The presence of secondary motions may thus lead to an erroneous decay law but in all the other experiments this motion remained insignificant; in general the energy of this motion represents less than 10 % of the total kinetic energy.

5. Determination of the law of spatial decay

The energy equation for the turbulence in the box when no interface is present is (neglecting the viscous transport term)

$$\frac{d}{dz}\left(\frac{1}{\rho}\overline{w'p'} + \frac{\overline{w'q^2}}{2}\right) + \epsilon = 0, \tag{1}$$

where ϵ is the rate of dissipation, w' the instantaneous vertical component of the turbulent velocity, q^2 the instantaneous turbulent energy and the bars indicate averages in a plane parallel to the grid at the level z. Since w/u remains constant (see figure 7) and since there is little doubt that the correlation coefficient remains constant the term $\overline{w'q^2} \propto u^3$. The pressure term may or may not be negligible but in any case is proportional to u^3. Taking $\epsilon = Au^3/l$ (Batchelor 1953, p. 103), (1) can be written in the form

$$du^3/dz = -Bu^3/l, \tag{2}$$

which has the solution (using $l = \beta z$)

$$u = u_0(z/z_0)^{-B/3\beta}. \tag{3}$$

This expression was first obtained by Thompson & Turner (1975) and used to correlate their results.

Bouvard & Dumas (1967) used a gradient-type diffusion of energy and for ϵ the expression $15\nu u^2/\lambda^2$, where λ is the Taylor microscale. This led to an elliptic integral for u^2 which was also in good agreement with the experimental results, in spite of the assumption that $Re_\lambda = u\lambda/\nu = $ constant and the constant eddy coefficient K_E, which are not supported by the experimental results for the perforated plate, at least not in the lower 25–30 cm. A simple power law is more attractive and analytically more convenient than an elliptic integral and in any case it fits the experimental results as well or better. If, furthermore, the restrictive assumptions $Re_\lambda = $ constant and $K_E = $ constant, implying $Re_l = $ constant, are made, one immediately obtains the power -1.

The horizontal r.m.s. turbulent velocities are plotted logarithmically as a function of distance (here z is measured from the virtual origin discussed in §4.3) in figure 10. The velocity at the level 30 cm was chosen as the reference velocity

since at greater distances the Reynolds number of the perforated-plate turbulence can be considered constant (see figure 9). In the experiments where no measurements were made at these positions an extrapolation according to the z^{-1} law was used. This presentation was chosen in order to emphasize the fact that the perforated-plate data are in good agreement with a z^{-1} law far away from the plate, where this turbulence can be considered to have planar homogeneity. It is evident from figure 10 that the perforated-plate results would be reasonably well represented by $u \propto z^{-\frac{3}{2}}$ as was proposed by Thompson & Turner (1975), but two regions of decay as discussed above seem to be more adequate. The grid results are on the whole better represented by $u \propto z^{-n}$ with n close to 1, including those of Thompson & Turner, which we have simply replotted (the extreme values only) from their figure 6 (a) using the same virtual origin (1 cm behind the grid, corresponding in our notation to $z_0' = \frac{1}{2}S + 1 \cdot 5$ cm) but a different reference velocity (we chose $u_r = 0 \cdot 08$ cm/s at $z_r = 30$ cm). Note that the slope is not affected by this choice of the reference velocity. Figure 10 shows the same behaviour as figure 9, i.e. the grid data for $M = 5$ cm and $S = 4$ cm as well as for $M = 10$ cm and $S = 9$ cm are well represented by a straight line of slope -1, whereas the data corresponding to $M = 10$ cm and $S = 4$ cm have a slope closer to $-1 \cdot 25$. Thompson & Turner's data are bounded by these slopes. A power-law fit is known to be very sensitive to a change in the virtual origin. The estimated uncertainty in z_0' is $\pm 0 \cdot 5$ cm, which affects the exponent by about $\pm 4 \%$.

The results obtained show that β and B individually vary with the grid geometry and the stroke but that B/β remains practically constant when the turbulence can be considered homogeneous, and has the value 3. It is of interest to get an expression for u_0 and z_0 in (3) in terms of the grid geometry, the frequency and the stroke. We have $u_0 = (fS) G(S/M)$, which according to figure 6 varies like $u_0 = (fS) CS^{\frac{1}{2}}$, where C is a function of M. For z_0 we have at our disposal S and M. When using M (which is equal to $5d$), (3) becomes for dimensional reasons

$$u/fS = CS^{\frac{1}{2}}M^{\frac{1}{2}}z^{-1}. \tag{4}$$

With a value for C of $2 \cdot 5 \times 10^{-1}$, Thompson & Turner's data are overestimated and our grid data underestimated by about 20%. For the perforated plate a different value of C must be chosen.

6. Mixing rate across a density interface

6.1. *Dependence of the mixing rate on the Richardson and Péclet number*

In the apparatus used for the present study the turbulent length and velocity scales are considerably greater than the corresponding scales obtained in Turner's (1968) apparatus. This aspect is of interest since it permits a systematic study of any possible influence of the length and/or velocity scales on the entrainment rate for a given Richardson number. This is not the purpose of this paper but entrainment rates have been measured for one grid geometry and stroke and are compared with Turner's (1973, p. 291) experimental data. The grid with $M = 10$ cm was used with $S = 4$ cm in these experiments and the corresponding turbulent
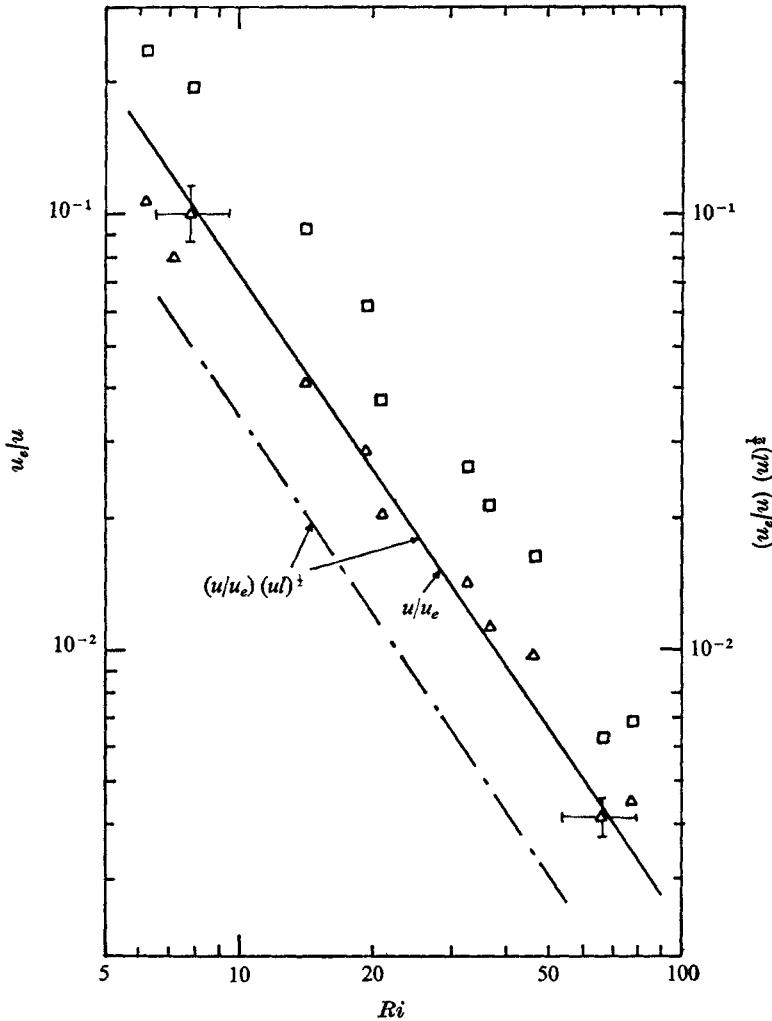
FIGURE 11. Variation of the non-dimensional entrainment velocity u_e/u with Richardson number. The salinity interface was 17·5 cm above the top position of the grid stirrer with $M = 10$ cm, $S = 4$ cm. $\triangle$, u_e/u; $\square$, $(u_e/u)\,(ul)^{\frac{1}{2}}$; ———, Turner's (1968) results u_e/u; — · —, Turner's (1968) results for $(u_e/u)\,(ul)^{\frac{1}{2}}$.

Reynolds numbers Re_l (proportional to the Péclet number) covered $230 \leqslant Re_l \leqslant 700$ as compared with $15 \leqslant Re_l \leqslant 30$ in Turner's experiments.

In figure 11, u_e/u as well as $(u_e/u)\,(ul)^{\frac{1}{2}}$, which is proportional to $(u_e/u)\,Pe^{\frac{1}{2}}$, are plotted as a function of Ri on a logarithmic scale. The visually determined depth of the turbulent layer was 17·5 cm, measured from the top position of the grid, and the Richardson number was calculated using the 'homogeneous' values of u and l at $z = 17·5$ cm $+ z_0'$ ($z_0' = 3$ cm for this stroke) given in figures 8 and 10. In general $u_e/u = F(Ri, Pe)$ and for very high Péclet numbers, Turner (1968) proposed

$$u_e/u \propto Ri^{-\frac{3}{2}}Pe^{-\frac{1}{2}}. \tag{5}$$

If (5) were correct the constant of proportionality obtained from the present

experiments should be the same as that in Turner's experiments. Here the change in Péclet number is due to a change in u and l and not a change in the molecular diffusivity. The results shown in figure 11 indicate, however, that when the Péclet number is high the entrainment rate is a function of Richardson number only. This supports Turner's (1973, p. 296) more recent suggestion that $u_e/u \propto Ri^{-\frac{3}{2}}$ in the large Péclet number limit.

6.2. *Turbulence characteristics in the presence of an interface*

The Richardson number defined in figure 11 is proportional to the global Richardson number Ri^* since Ri has been defined using the homogeneous u and l scales. It is, therefore, no surprise that $u_e/u \propto Ri^{-\frac{3}{2}}$. Long (1975) suggested that the Ri^{-1} law, which is supported by energy arguments, is more fundamental and that the $Ri^{-\frac{3}{2}}$ behaviour is based on a false hypothesis, namely that $u \propto f$. Long showed that in order to account for the difference it is only necessary that

$$u/f \propto Ri^{*-\frac{1}{6}}, \tag{6}$$

which leads to $u \propto f^{\frac{4}{3}}$ when the other variables are held constant. In fact a very weak density gradient exists in the mixed layer (Wolanski & Brush 1975) but it is hard to believe that this could have a dynamic effect.

To test (6) measurements of u were attempted in the presence of a very stable salinity interface. In these experiments the probe was positioned at either 9 or 18 cm from the top of the grid and the height of the interface was allowed to vary with respect to the probe, i.e. no fluid was withdrawn. Generally the probe was kept in the fully turbulent region, which was estimated to extend up to $H - h$ (see figure 12 for definition), where h was taken as $1 \cdot 5l$ according to Crapper & Linden (1974) and the values of h indicated correspond to the position $H - \frac{1}{2}h$. Figure 12 shows a logarithmic plot of u as a function of the stirrer frequency. The experimental scatter is large mainly because of probe drift and deterioration of the probe in a rather short time when used in water of high salinity.† Nevertheless, the group of experimental points is best represented by $u \propto f$, although some individual runs ($z' = 9$ and 18 cm, $H = 24$ cm) would not disagree with a behaviour $u \propto f^{\frac{4}{3}}$. Since $H_0 > H$ the product $\Delta\rho H$ does not remain constant when H changes during a run and we should have plotted $(\Delta\rho H)^{\frac{1}{6}}u = F(f)$, but this correction is absorbed in the experimental scatter. Owing to this scatter the conclusion to be drawn is not definitive but since the slope $\frac{4}{3}$ is an upper bound to the experimental points there seems to be little doubt‡ that $u \propto f$ and hence $u_e/u \propto Ri^{-\frac{3}{2}}$. The homogeneous values of u and l are thus representative of the values near an interface.

The thickness of the interface was measured by means of a laser beam which was horizontally traversed through the density interface. The importance of the

---

† Conical probes suited only for use in fresh water were used. Measurements were nevertheless possible because calibration was easy and could be repeated before and after each run.

‡ After the manuscript was sent to the editor, these measurements were repeated with special probes which showed no drift when properly grounded. The results confirmed that $u \propto f$.
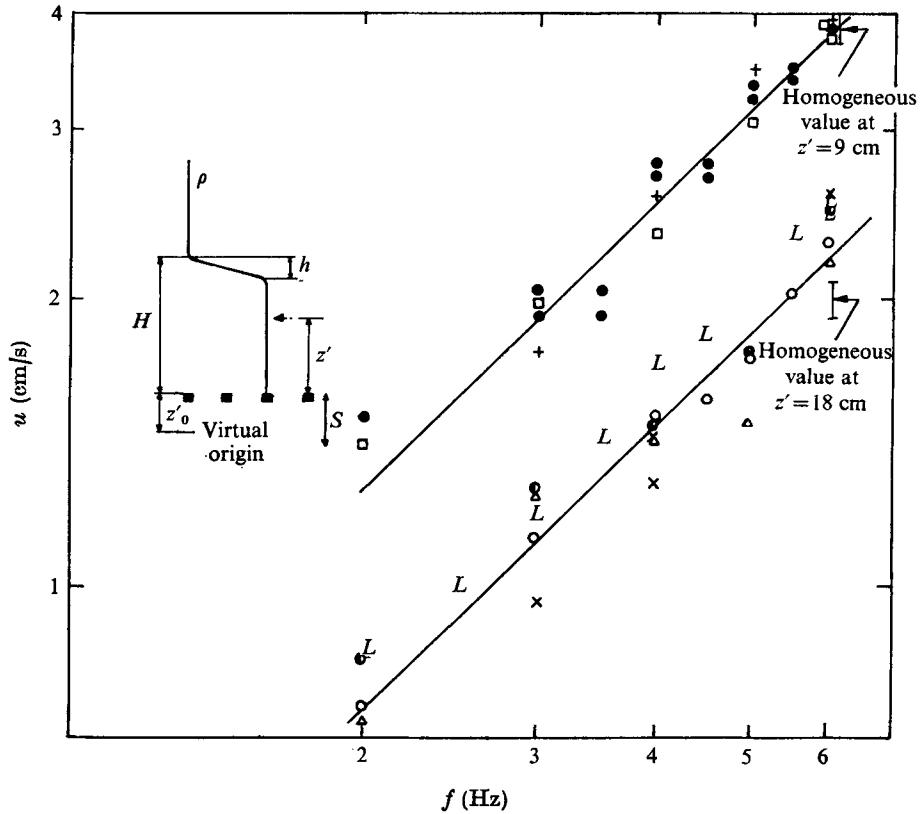
FIGURE 12. R.m.s. horizontal velocity u at $z = 12$ and 21 cm plotted logarithmically against grid oscillation frequency with a density interface at various positions H. The laser-anemometer results (marked L) obtained without an interface are included for comparison.

z' (cm)		H (cm)	h (cm)	$\Delta\rho/\rho$ (%)
○	18	31·5	7·2	0·6
□	9	17–19	4·2–4·6	1·4
△	18	21·5–25	5·1–5·9	0·7
+	9	24	5·7	3·6
×	18	24	5·7	3·6
●	9	14–19	3·6–4·6	0·75
◑	18	21·5	5·1	1·5
L	13	—	—	0

density gradient can be inferred from the bending of the laser beam. It was found necessary to distinguish between static and dynamic interface thicknesses h_s and h_d respectively. Both were measured at two values of Ri, differing by a factor of 10. The thickness h_s was determined after the stirrer had been stopped and the turbulent motion had calmed down. It was found that $h_s \simeq l$ for both values of Ri. The thickness h_d was measured while the stirrer was in action and in this case a clear dependence on Ri is observed. The eddies which are projected against the interface from the denser turbulent layer penetrate the lighter non-turbulent layer and then bounce back. This mechanism, observed by Linden

(1973) when projecting vortex rings against an interface, results in large density variations over a thickness $h_d > h_s$. The results seem to indicate that $(h_d - h_s)/h_s \propto Ri^{-1}$.

The entrainment velocity in the limiting case $Ri \to 0$ is of interest in the evaluation of the time needed for turbulence which is generated at the surface by a gust to reach the thermocline. Such experiments have been performed with the perforated plate for Richardson numbers of the order of 0·05. The ratio u_e/u was found to vary between 0·8 at 40 cm from the top position of the plate to 1·4 at 23 cm. Far away from the stirrer (beyond 30 cm; see figure 9) the turbulence is more nearly isotropic and $u_e \approx u$, which agrees with the values indicated by Turner (1973, p. 298).

7. Discussion and conclusion

It has been shown that an oscillating grid of appropriate geometry is capable of generating nearly isotropic turbulence without a mean flow. The spatial decay of the turbulent energy is governed by $\overline{q^2} \propto z^{-n}$ with $n \simeq 2$, and since the integral scale increases with distance as $l = \beta z$, the Reynolds number Re_l remains approximately constant during the decay. The turbulence generated by the perforated plate used by Bouvard & Dumas (1967), on the other hand, is on the whole better represented by $\overline{q^2} \propto z^{-3}$, but it seems more appropriate to consider two zones, one near the plate where $Re_l \propto z^{-\frac{1}{2}}$ and the other far away where $Re_l = \text{constat}$. This behaviour is most probably a result of the high solidity of the plate ($> 60\%$), which causes an unstable regime (jet switching) similar to what is observed behind fixed grids of high solidity ($> 40\%$; see Corrsin 1963).

The influence of the stroke on the characteristics of the turbulence also becomes clear from an examination of figure 8, which shows that the integral scale is proportional to the mesh size only when the stroke is of the same order ($S/M \geqslant 0·8$). One conclusion to be drawn is that, in Turner's equipment, where S was kept constant at 1 cm, use of a grid with $M = 1·5$ cm and $d = 0·3$ cm operated at a frequency increased by $3^{\frac{1}{2}}$ [see (4)] would generate turbulence which had the same u and l as those measured by Thompson & Turner (1975) but with considerably improved planar homogeneity.

The measured turbulent length and velocity scales have been related to the entrainment rate across a salinity interface for the grid with $M = 10$ cm for $S/M = 0·4$. The results obtained are represented by $u_e/u \propto Ri^{-\frac{3}{2}}$ as is to be expected. It was, however, not at all clear that the constant of proportionality would remain independent of the turbulent length and velocity scale. For an identical diffusivity the Péclet number in the present experiments was about 20 times larger than in Turner's (1968) experiments, but the constants of proportionality are identical as may be seen in figure 11. This result is of some importance since it implies that when the Péclet number is large the mixing process is a function of the Richardson number only and (5) is not valid. An alternative expression to that proposed by Turner (1968) is

$$u_e/u = Ri^{-\frac{3}{2}}(K_1 + K_2(Ri/Pe)^{\frac{1}{2}}), \tag{7}$$

which gives for large Péclet numbers $u_e/u = K_1 Ri^{-\frac{3}{2}}$ and for small Péclet numbers $u_e/u = K_2 Ri^{-1} Pe^{-\frac{1}{2}}$. K_1 and K_2 are constants. No systematic study of the dependence of the entrainment rate on Péclet number at low Péclet numbers has been carried out but such a dependence may be inferred from the work of Crapper & Linden (1974). They showed that at low Péclet numbers ($Pe < 200$) the diffusive flux in the interface is equal to the measured flux, which means that the buoyancy flux q is proportional to κ/h, where κ is the diffusivity and h the interface thickness. Their experimental data are not inconsistent with $h/l \propto Pe^{-\frac{1}{2}}$, which leads to $q/u \propto \Delta/b Pe^{-\frac{1}{2}}$, Δ/b being the buoyancy jump across the interface.

Now returning to the case of high Péclet number, the expression (7) implies that the $Ri^{-\frac{3}{2}}$ form is of fundamental importance to the entrainment rate in the buoyancy-controlled turbulent regime, and this seems to be widely accepted (Turner 1973, p. 296). But, as Long (1975) argued, it is not evident that a density interface would have no effect on the turbulence characteristics at a position near to it. The results presented in figure 12 indicate, however, that the r.m.s. horizontal turbulent velocity does remain proportional to the frequency but that there is a tendency for this velocity component to be slightly larger than the corresponding homogeneous value.

According to Wolanski & Brush's (1975) experimental results neither form is of a fundamental nature. These authors correlated their results with $u_e/u_* \propto Ri^{*-n}$ with n a function of the Prandtl or Schmidt number. In their experiments the diffusivities ranged from 10^{-3} cm²/s for heat to apparently about 10^{-9} cm²/s for a clay suspension and correspondingly n varied from 1 to about 4. If Long's reasoning is extended to these results the r.m.s. turbulent velocity near the clay interface would have to vary like f^3. This would mean that the density gradient in the quasi-homogeneous layer is a function of the diffusivity, which is difficult to accept. The curious results of Wolanski & Brush are likely to be connected with the use of suspensions (the sugar and salt results hardly differ) rather than solutions and it is possible that the mechanism of generation is modified by non-Newtonian behaviour. In conclusion we may say that ultimately these discrepancies can be resolved only by more detailed information on the entire flow structure, particularly that near the interface.

REFERENCES

BAINES, W. D. 1975 Entrainment by a plume or jet at a density interface. *J. Fluid Mech.* **68**, 309–320.

BATCHELOR, G. K. 1953 *Homogeneous Turbulence*. Cambridge University Press.

BOUVARD, M. & DUMAS, H. 1967 Application de la méthode du fil chaud à la mesure de la turbulence dans l'eau. *Houille Blanche*, **22**, 257–278, 723–733.

CORRSIN, S. 1963 Turbulence: experimental methods. *Handbuch der Physik*, vol. VIII/2, *Strömungsmechanik*, II, pp. 524–587. Springer.

CRAPPER, P. F. & LINDEN, P. F. 1974 The structure of turbulent density interfaces. *J. Fluid Mech.* **65**, 45–63.

KATO, H. & PHILLIPS, O. M. 1969 On the penetration of a turbulent layer into a stratified fluid. *J. Fluid Mech.* **37**, 643–655.

LINDEN, P. F. 1973 The interaction of a vortex ring with a sharp density interface: a model for turbulent entrainment. *J. Fluid Mech.* **60**, 467–480.

LINDEN, P. F. 1975 The deepening of a mixed layer in a stratified fluid. *J. Fluid Mech.* **71**, 385–405.

LISMONDE, B. 1976 Les anémomètres à laser. Etude de leurs caractéristiques. Réalisation de prototypes. Thèse de Docteur-Ingénieur, Université de Grenoble.

LONG, R. R. 1975 The influence of shear on mixing across density interfaces. *J. Fluid Mech.* **70**, 305–320.

RESCH, F. J. & LEUCHTHEUSSER, H. J. 1972 Mesures des tensions de Reynolds dans le ressaut hydraulique. *J. Hydraul. Res.* **10**, 409–430.

ROUSE, H. & DODU, J. 1955 Diffusion turbulente à travers une discontinuité de densité. *Houille Blanche*, **10**, 522–532.

THOMPSON, S. M. & TURNER, J. S. 1975 Mixing across an interface due to turbulence generated by an oscillating grid. *J. Fluid Mech.* **67**, 349–368.

TOLY, J.-A. 1975 Diffusion turbulente d'énergie et de masse avec application au problème de la thermocline. Thèse de Docteur-Ingénieur, Université de Grenoble.

TURNER, J. S. 1968 The influence of molecular diffusivity on turbulent entrainment across a density interface. *J. Fluid Mech.* **33**, 639–656.

TURNER, J. S. 1973 *Buoyancy Effects in Fluids*. Cambridge University Press.

WOLANSKI, E. J. & BRUSH, L. M. 1975 Turbulent entrainment across stable density step structures. *Tellus*, **27**, 259–268.

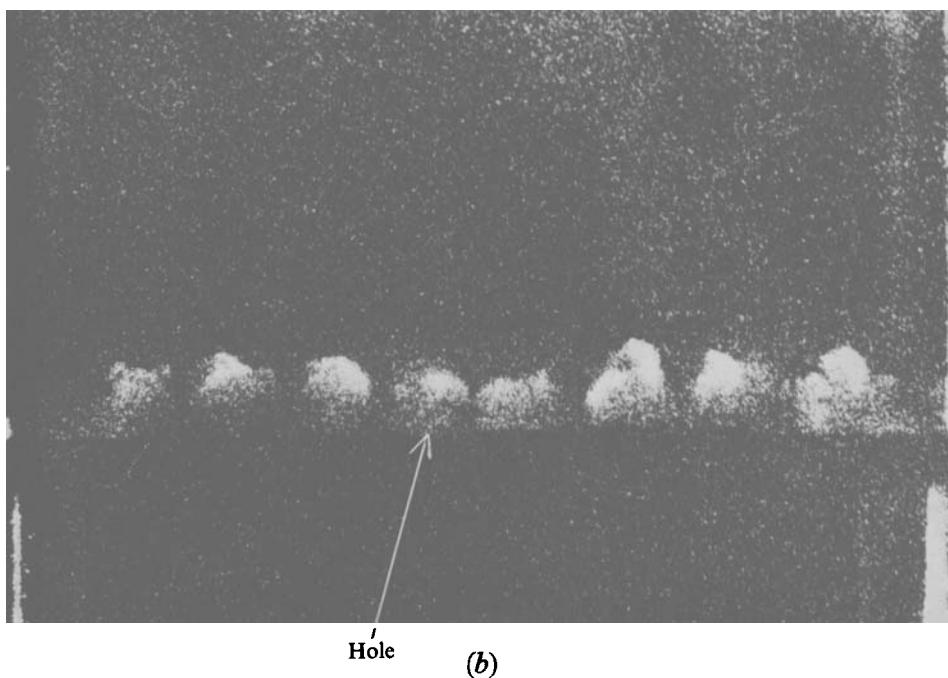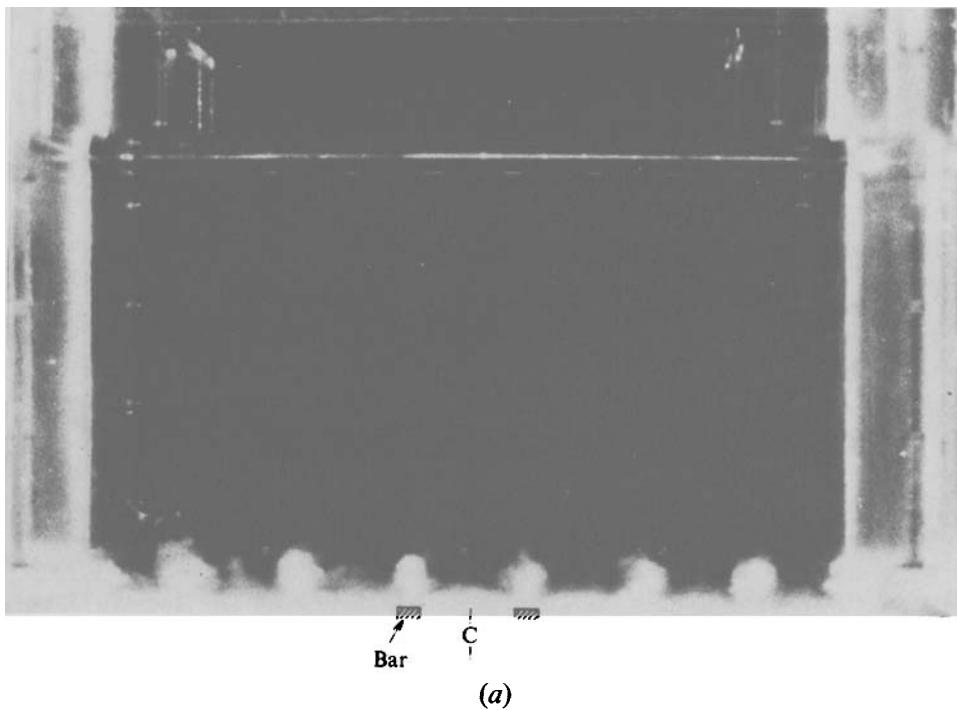WU, J. 1973 Wind-induced turbulent entrainment across a stable density interface. *J. Fluid Mech.* **61**, 275–287.

FIGURE 2. Photographs showing the apearance of the wakes and jets when the stirrer is set in motion (a) for a grid of square bars with $M = 10$ cm and (b) for the perforated plate. Note that in (a) the turbulence is above the bars, whereas in (b) the jets are centred above the holes.